Korean J. Chem. Eng., 40(12), 2906-2913 (2023)
DOI: 10.1007/s11814-023-1485-0

pISSN: 0256-1115
eISSN: 1975-7220

Enhanced photocatalytic activity of $TiO_2/Ca_{12}Al_{14}O_{33}$ in NO removal

Ji Hye Park*, Min Woo Hong, Wathone Oo**, Jung Joon Park***, Hee Ju Park****, and Kwang Bok Yi*,†**

*Department of Chemical Engineering Education, Chungnam National University, 99 Daehak-ro, Yuseong-gu, Daejeon 34134, Korea
**Graduate School of Energy Science and Technology, Chungnam National University, 99 Daehak-ro, Yuseong-gu, Daejeon 34134, Korea
***Department of Structural Engineering Research, Korea Institute of Civil Engineering and Building Technology, 283 Goyangdae-ro, Ilsanseo-gu, Goyang-si, Gyeonggi-do 10223, Korea
****BENTECHFRONTIER Co., Ltd. 77 Yongbong-ro, Buk-gu Gwangju 61186, Korea
(*Received 2 January 2023 • Revised 13 April 2023 • Accepted 1 May 2023*)

Abstract−TiO_2 supported on $Ca_{12}Al_{14}O_{33}$ (Mayenite) was synthesized and investigated for use as a photocatalytic concrete material. TiO_2/Mayenite (TiO_2/M) catalysts were prepared with varying TiO_2 loading amounts (1-20 wt%). The photocatalytic activity of the catalysts was measured using the ISO standard NO removal test. TiO_2/M catalysts exhibited significantly enhanced photocatalytic activities compared to pure TiO_2, with the NO removal efficiency increasing as TiO_2 loading increased up to 10 wt% and then decreasing with further loading of TiO_2. The NO removal rate of the TiO_2/M catalyst, which contained 10 wt% TiO_2, was 8.72 μmol (equivalent to 350 μmol/m^2·h). X-ray photoelectron spectroscopy (XPS) analysis suggested that oxygen on the TiO_2/M catalysts with low TiO_2 loading exists in the form of Ti-OH rather than TiO_2. This study focuses on the formation of Ti-OH on the catalyst surface, which is promoted by the unique crystal structure of Mayenite that supplies oxygen ions and electrons to the TiO_2 layer. The NO removal efficiency of the catalysts was found to be dependent on the interaction between TiO_2 and Mayenite. Overall, this study demonstrates the potential of TiO_2/Mayenite for use as a highly effective photocatalytic concrete material, with the unique properties of the Mayenite support playing a critical role in enhancing the photocatalytic activity of the catalyst.

Keywords: Photocatalyst, Titanium Dioxide (TiO_2), Mayenite ($Ca_{12}Al_{14}O_{33}$), Nitrogen Oxides, Particulate Matter

INTRODUCTION

NO_x is recognized as one of the primary pollutants responsible for causing severe air pollution, so controlling its emissions remains a significant challenge due to its wide and diverse sources [1,2]. Particularly, NO_x emitted from vehicles with internal combustion engines causes photochemical smog and fine dust in metropolitan areas, heavily-trafficked roads, and tunnels [3-5]. Various technologies are available to remove NO_x, including chemical adsorption, electrochemical methods, selective catalytic reduction (SCR), and photocatalysis [6-11]. Among these, photocatalysis has been investigated as a promising solution for reducing vehicle-generated NO_x emissions by incorporating photocatalysts into construction materials used for road pavements, tunnels, bus stops, and noise barriers in residential areas [12-14]. Titanium dioxide (TiO_2) is a popular and technically advanced photocatalyst that is highly stable and cost-effective. However, it is not without drawbacks, including electron-hole pair recombination and poor pollutant adsorption capacity [15-17]. Many studies have sought to address these issues by modifying the TiO_2 surface with noble metals or incorporating semiconductor materials during preparation to improve its electrochemical properties [18,19]. Since TiO_2 itself lacks adsorption ability, porous materials with high surface areas, such as zeolites, activated carbon, and silica, have been used as support materials to provide numerous active sites and promote fast mass transfer [20-24]. In addition to enhancing the reactivity and activity of TiO_2, the affinity of TiO_2 with cementitious materials must also be considered when incorporating it onto the surfaces of roads or building walls for NO_x removal. Recent attempts have focused on increasing the reactivity and dispersal of TiO_2 in concrete using medium supports for TiO_2 [25-27]. Yousefi et al. [25] reported that a coating slurry was produced by mixing TiO_2 nanoparticles with a $Ca(OH)_2$ solution and focused on adjusting the ratio of TiO_2 nanoparticles to $Ca(OH)_2$ to prevent nanoparticle agglomeration. Li et al. [26] prepared a TiO_2-based pigment for building walls that was tested for its ability to remove NO. Additionally, TiO_2 was physically mixed with calcium aluminate cement (CAC) and tested for NO removal. Nicolás et al. [27] studied the photocatalytic activity of commercial TiO_2 applied to two types of calcium aluminate cement, iron-rich and non-rich cement. They also compared the activity according to the TiO_2 content.

The photocatalytic reaction of NO_x occurs according to the following Eqs. (1)-(7) [27]:

$$TiO_2+hv\rightarrow e^-+h^+ \quad (1)$$

$$H_2O+h^+\rightarrow H^++OH\bullet \quad (2)$$

$$O_2+e^-\rightarrow O_2\bullet^- \quad (3)$$

†To whom correspondence should be addressed.
E-mail: cosy32@cnu.ac.kr

$$NO+O_2\bullet^- \rightarrow NO_3^- \quad (4)$$

$$NO+OH\bullet \rightarrow HNO_2 \quad (5)$$

$$HNO_2+OH\bullet \rightarrow NO_2+H_2O \quad (6)$$

$$NO_2+OH\bullet \rightarrow NO_3^-+H^+ \quad (7)$$

Yao et al. [28] used hydroxyapatite (HAp) as a support for a TiO_2-based catalyst, and they claimed that the photocatalytic activity of TiO_2/HAp composites was enhanced due to stronger chemisorption of NO, higher separation efficiency, and faster transfer of photogenerated electron-hole pairs. To effectively utilize photocatalysts on medium supports in construction materials, it is crucial that TiO_2 particles are evenly dispersed and immobilized on a surface that is accessible to light. The medium support should not chemically bind with TiO_2 and interfere with its photocatalytic activity. Additionally, the medium support should have an affinity with the materials that make up concrete to prevent detachment or washing away of the TiO_2 loaded support with aging.

In this study, we selected Mayenite ($Ca_{12}Al_{14}O_{33}$, also known as $12CaO{\cdot}7Al_2O_3$, C12A7), as the medium support for photocatalyst preparation. Hosono et al. [29] reported that the crystals of $Ca_{12}Al_{14}O_{33}$ possess an inversed zeolitic nature with anion accommodation properties. Kim et al. [30] and Li et al. [31] also observed these features of $Ca_{12}Al_{14}O_{33}$ and used it to enhance the multi-cycle stability of high-temperature CO_2 absorbents. We hypothesized that $Ca_{12}Al_{14}O_{33}$ would behave as an oxygen-vacancy possessing material that could improve the transport of electrons in photocatalytic activity. Furthermore, $Ca_{12}Al_{14}O_{33}$ is also one of the main components in cementitious materials. In a previous study, we briefly reported on the possibility of using $Ca_{12}Al_{14}O_{33}$ as a support material for TiO_2 photocatalysts [32]. However, that study only focused on the preparation of TiO_2 particles and had limited information on the supporting material. In this study, we report in detail on the effects of $Ca_{12}Al_{14}O_{33}$ as a support material on the photocatalytic activity of TiO_2 catalysts, including our preparation methodology.

EXPERIMENTAL SECTION

1. Synthesis of Composites

1-1. Mayenite-$Ca_{12}Al_{14}O_{33}$

$CaCO_3$ (98.5%, Duksan Reagents) and Al_2O_3 (99.0%, Samchun Reagents) were used as precursors in a 12 : 7 mole ratio. The precursors were placed in a 5 L custom-made ball mill with ceramic balls of 10 mm diameter and milled at room temperature for 24 hours. The resulting powder was collected and calcined at 1,473 K in air for 24 hours. After cooling to room temperature, the calcined material was crushed and sieved.

1-2. TiO_2 Supported Mayenite

To synthesize TiO_2 loaded Mayenite (TiO_2/M), titanium(IV) isopropoxide (TTIP, Sigma Aldrich) is first mixed with isopropyl alcohol (IPA, Sigma Aldrich). Then, an aqueous urea solution containing urea in the same mole ratio as TTIP is gradually added to the mixture of TTIP and IPA. The resulting solution is stirred for 30 minutes at room temperature. Next, pre-synthesized Mayenite powder is added to the sol-gel solution with vigorous mixing and aged for 2 hours. The sol-gel mixture is then dried at 373 K for 24 hours in a convection oven. After calcination at 773 K for 3 hours, TiO_2/M is obtained.

The amount of TTIP is carefully calculated to result in designated TiO_2 loading values in the range of 1 to 20 weight percent (wt%). TiO_2 loadings of 1, 3, 5, 10, 15, and 20 wt% are selected. The prepared samples are designated by the TiO_2 loading percentage, for example, 3-TiO_2/M represents 3 wt% of TiO_2 loaded on Mayenite.

1-3. TiO_2

The reference material of TiO_2 powder was also prepared using the same method as for the TiO_2/M catalyst, with the exception of omitting the addition of Mayenite. The TiO_2 powder was synthesized as described in our previous study [32].

2. Characterization

The BET surface area and BJH pore size distribution of the TiO_2/

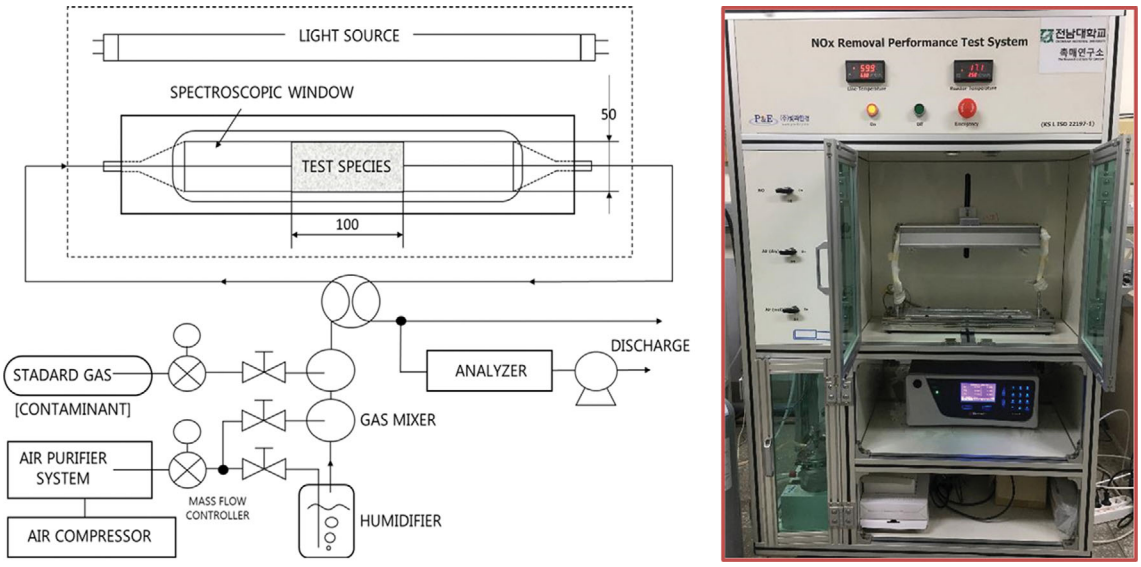

Fig. 1. Schematic diagram and photo of photocatalytic NO removal test apparatus.

M samples were determined using BELSORP-miniX (Microtrac-BEL) by measuring N_2 physisorption isotherms at 77 K. Prior to N_2 adsorption, the samples were dried at 473 K for 4 hours under vacuum to remove retained gases and water. The crystal structures of the catalysts were examined by X-ray diffraction (XRD) using a D8 ADVANCE instrument with a scanning rate of 1°/min from 10 to 90° and a scanning step size of 0.02°. The elemental analysis of the TiO_2/M samples was conducted using a wavelength dispersive X-ray fluorescence spectrometer (WD-XRF, ZSX Primus II/Rigaku). X-ray photoelectron spectroscopy (XPS) was employed to analyze the chemical state of the samples, using a K-Alpha$^+$ instrument (Thermo scientific) with an Al X-ray source, a spot size of 650 μm, and an energy step size of 0.1 eV. The hydrocarbon C 1s line at 284.8 eV from adventitious carbon was used for energy referencing in XPS spectrum.

3. NO Removal Test

The photocatalytic properties of the samples were evaluated using a custom-designed apparatus (Fig. 1) in accordance with the protocol specified in ISO 22197-1. The sample frame (100 mm× 50 mm) was loaded with 3 g of TiO_2 and TiO_2/M powder and placed inside the sample chamber that was positioned under the light source. After N_2 adsorption, 1 ppm NO in an air stream at a flow rate of 3 L·min^{-1} was introduced into the sample chamber and allowed to reach equilibrium in the dark. The NO concentration in the effluent was monitored until it matched the inlet gas concentration. Subsequently, UV light with an intensity of 10 W/m^2 was turned on and the volumetric concentration of NO and NO_2 in the effluent gas was monitored for 5 h. Concentrations of NO and NO_2 were determined by chemiluminescence (Ecotech, Serinus 40) at the outlet of photo reactor. The temperature and relative humidity were maintained at 25 °C and 50%, respectively, throughout the experiment.

RESULTS AND DISCUSSION

To improve the compatibility of the TiO_2 precursor solution with the Mayenite powder without the addition of water, the quantities of the ingredients were adjusted, as shown in Table 1. The concentration of the aqueous urea solution was maintained at 2 M, and the molar amount of urea was kept the same as that of TTIP for each batch, based on the target TiO_2 loading. However, the amount of IPA was kept constant at 51.27 g. This ensured that Mayenite could be effectively mixed with TTIP and the urea solution. We discovered that adding water to improve the dispersion of Mayenite powder in the sol-gel solution could significantly reduce the catalytic performance of the TiO_2/M sample. We will report on the impact of additional water on the catalytic activity of TiO_2/M separately in the near future. This study focuses on the mechanism of the photocatalytic reaction in the presence of Mayenite support. The XRD patterns of the TiO_2/M catalysts are shown in Fig. 2. The patterns were almost identical to the well-developed Mayenite crystal structure. A signature peak of TiO_2 (anatase type) was observed in all samples at around 25.5°. Its intensity increased with increasing TiO_2 loading. The peaks of Mayenite decreased as the TiO_2 loading increased, most likely due to the coverage of TiO_2 particles on the surface of Mayenite. The TiO_2 powder (not shown in Fig. 2) used as a reference was identified as the anatase form [32]. According to Nicolás et al. [27], when TiO_2 is added to calcium aluminate cement (CAC), TiO_2 peaks are formed and the anatase structure can be confirmed, but the peaks are not clearly visible due to the large amount of CAC. These results are similar to the XRD patterns of the TiO_2/M catalysts, and we performed XRF analysis to analyze the elements of the TiO_2/M catalysts, the results of which are shown in Table 2. It was confirmed that TiO_2 increases as the

Table 1. The amount of ingredients in preparation of TiO_2/M catalysts (unit: g, 10 g catalyst basis)

TiO_2 [wt%]	TiO_2	TTIP	IPA	Urea	H_2O
1	0.1	0.36	51.27	0.08	0.56
3	0.3	1.07	51.27	0.24	1.66
5	0.5	1.78	51.27	0.40	2.77
10	1	3.57	51.27	0.79	5.56
15	1.5	5.34	51.27	1.19	8.32
20	2	7.11	51.27	1.58	11.08

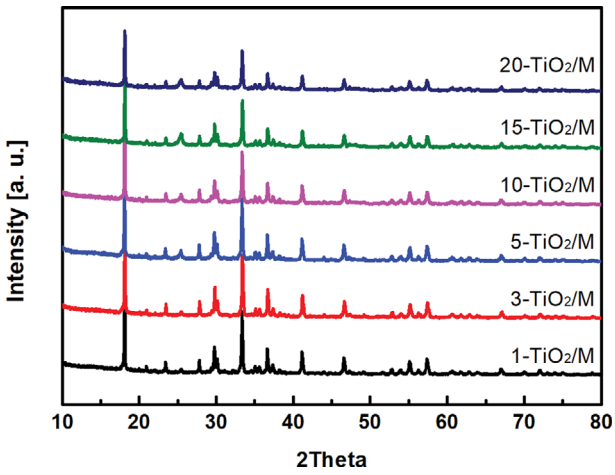

Fig. 2. XRD patterns of TiO_2/M catalyst prepared by the modified method.

Table 2. XRF analysis results of TiO_2/M catalysts (unit: wt%)

Sample	1-TiO_2/M	3-TiO_2/M	5-TiO_2/M	10-TiO_2/M	15-TiO_2/M	20-TiO_2/M	TiO_2(500)
TiO_2	3.0297	6.2867	14.4892	28.7924	38.4378	47.6988	98.9656
Al_2O_3	20.6700	19.2019	16.7121	15.6935	12.7394	8.6281	0.0113
CaO	74.9063	73.1514	67.1344	54.1193	47.4187	41.5800	0.2300
Others	1.3940	1.3600	1.6643	1.3948	1.4041	2.0931	0.7931

amount of TiO_2 increases, and that calcium and aluminum are present with some other impurities.

BET analysis results in Table 3 show that the specific surface areas of all samples, including TiO_2 powder, were significantly low. Although the specific surface areas of the TiO_2/M catalysts show an increasing trend as TiO_2 loading increased, it is uncertain if photocatalytic performance is affected by differences in surface area due to the low values. Photocatalytic reactions are confined to the catalyst surface where light can reach, making pore volume and pore diameter more relevant indicators. The formation of TiO_2 particles on the Mayenite surface developed mesopores, resulting in a slight increase in specific surface area, which is supported by SEM analy-

Table 3. BET analysis results of TiO_2/M catalysts

Sample	Surface area (m^2/g)	Pore volume (cm^3/g)	Pore diameter (nm)
1-TiO_2/M	6.8	0.05	29.1
3-TiO_2/M	7.4	0.07	39.4
5-TiO_2/M	10.4	0.09	34.7
10-TiO_2/M	14.3	0.13	37.1
15-TiO_2/M	27.0	0.13	19.6
20-TiO_2/M	42.6	0.19	18.0
TiO_2(500)	20.0	0.14	29.2

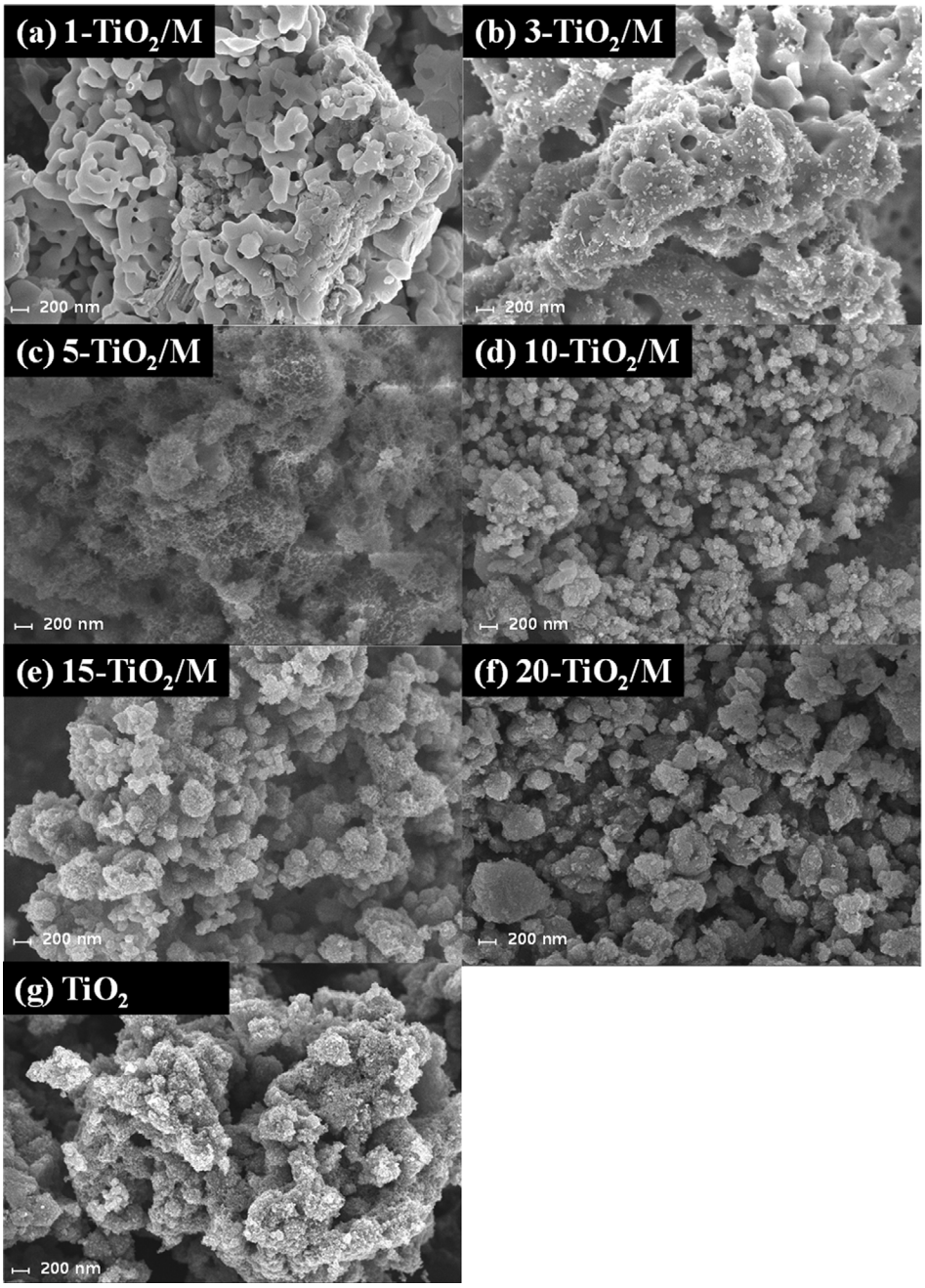

Fig. 3. SEM images of TiO_2/M catalysts prepared by the modified method.

sis results shown in Fig. 3. The 1-TiO_2/M sample consisted of peanut-like particles, presumably the Mayenite, connected to each other with smooth surfaces, and small debris was observed in limited regions. As TiO_2 loading increased, flake-like TiO_2 particles were observed on the Mayenite surface, forming a web and eventually agglomerating into round particles of around 100 nm in size in 10-TiO_2/M. If the Mayenite's role in photocatalytic activity is correct, there may be an optimum TiO_2 loading amount for the best NO removal efficiency. If the coverage of TiO_2 particles on Mayenite is too low, the promotion effect of Mayenite will be limited. On the other hand, if the coverage is too high, a thick layer of TiO_2 may be formed, preventing UV light from reaching the Mayenite layer and making catalytic performance dependent only on TiO_2 particles themselves.

The results of nitrogen oxide (NO) removal tests, in Fig. 4, are consistent with our initial assumptions. The trends of NO removal rate as a function of TiO_2 loading were similar for both 60 and 300 minutes of ultraviolet (UV) irradiation. For 300 minutes of UV irradiation, the NO removal rate for 1-TiO_2/M was approximately 1.45 μmol, equivalent to 56 μmol/m^2·h. As the TiO_2 loading increased, the NO removal rate also increased until it reached 8.72 μmol for 10-TiO_2/M, which is equivalent to 350 μmol/m^2·h. However, for 15-TiO_2/M and 20-TiO_2/M, the NO removal rates were 6.52 μmol and 6.53 μmol, respectively, lower than that of 10-TiO_2/M. These findings challenge our initial hypothesis that the oxygen vacancies in Mayenite contributed to the NO removal.

One possible explanation for the reverse trend of NO removal rate at high TiO_2 loading is the electron-hole recombination, which can occur when the TiO_2 loading is large. This phenomenon has been previously reported by Rhee et al. [33] in their investigation of NO removal efficiency of TiO_2 powder in cementitious materials. They found a similar reverse trend of NO removal efficiency as the TiO_2 loading increased, which they attributed to the electron-hole recombination. However, they did not observe this behavior when TiO_2 was mixed with mortar instead of cement paste, and they used physical mixing instead of the impregnation method used in our study. Moreover, the reference material, pure TiO_2 powder, showed a lower NO removal rate of 5.42 μmol after 300 minutes of UV irradiation compared to most TiO_2/M samples. Thus, we conclude that the explanation of oxygen vacancies in Mayenite as the cause of NO removal is more plausible than the electron-hole recombination hypothesis.

The promotion of oxygen vacancies on TiO_2 has been extensively investigated in previous studies. For example, Tan et al. [34] reported that oxygen vacancies on N-doped TiO_2 can enhance oxygen diffusion in the TiO_2 lattice, resulting in increased NO removal efficiency. Nakamura et al. [35] found that heat treatment of TiO_2 created an oxygen vacancy state between the valence and conduction bands in the TiO_2 band structure, leading to highly selective NO removal. In contrast, Eskandarloo et al. [36] synthesized a TiO_2/CeO_2 hybrid photocatalyst for NO removal, and claimed that a smaller band gap of CeO_2 enhanced electron-hole pair separation in TiO_2 by reducing recombination. In this study, however, the improved NO removal efficiency is attributed to the oxygen vacancies and O^{2-} ions trapped in the Mayenite cage. These characteristics of Mayenite have been well-established and thoroughly investigated by numerous researchers [29,30,37]. Our assumption is further supported by an examination of the catalyst's element oxidation states. Fig. 5 shows typical local XPS scans of the TiO_2 powder, revealing only one oxidation state in the Ti 2p peak (~458.7

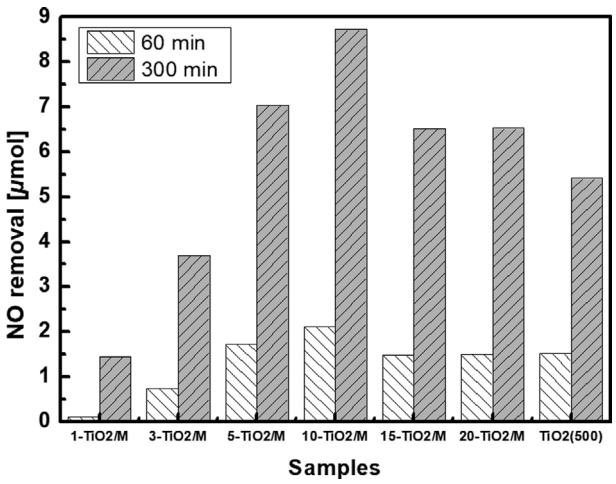

Fig. 4. NO removal test results of TiO_2/M catalysts and pure TiO_2 powder.

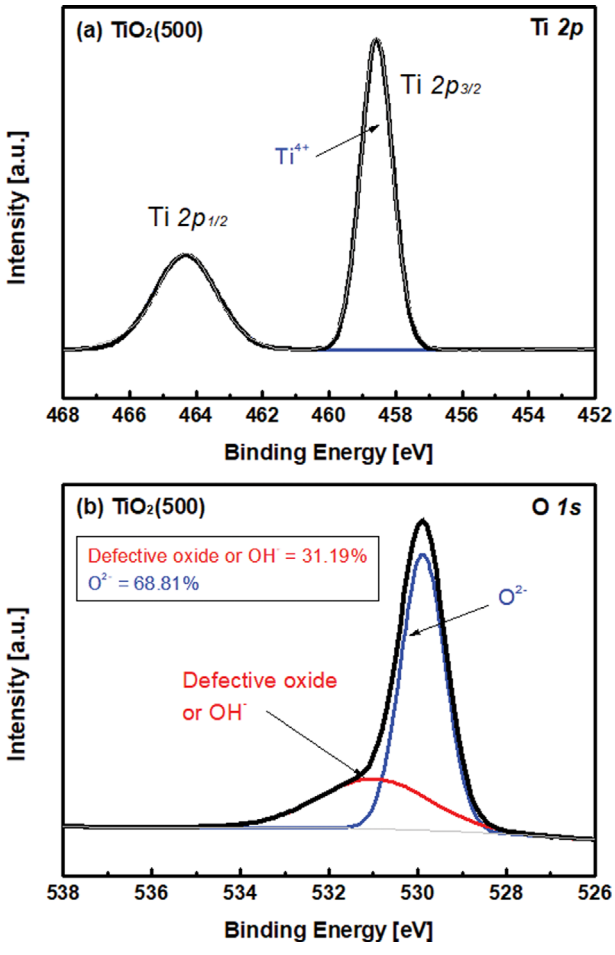

Fig. 5. XPS analysis result of pure TiO_2 powder.

eV) based on the spin-orbit coupling of the Ti $2p_{3/2}$ and $2p_{1/2}$ peaks. However, fitting of the O 1s peaks indicates two oxygen states. The first (~529.7 eV) is associated with lattice oxygen coupled with Ti atoms, while the second (~531.1 eV) is attributed to defective oxygen or hydroxide [38]. These titanium hydroxides or suboxide species typically form on the surface due to broken and dangling bonds from oxygen that need to be terminated [39]. Surface hydroxyls have been shown to play a crucial role in the NO_x removal process [40,41].

It is evident that the oxygen species in TiO_2 form are predominant on the surface of pure TiO_2 powder, rather than those in the Ti-OH form. However, the O 1s peaks of TiO_2/M samples exhibit distinctive features in Fig. 6 due to the presence of Mayenite, $Ca_{12}Al_{14}O_{33}$. The O 1s peaks of all TiO_2/M samples were deconvoluted into two peaks. The first peaks correspond to bi-valence oxygen, similar to those found in pure TiO_2, while the second peaks at around ~531.2

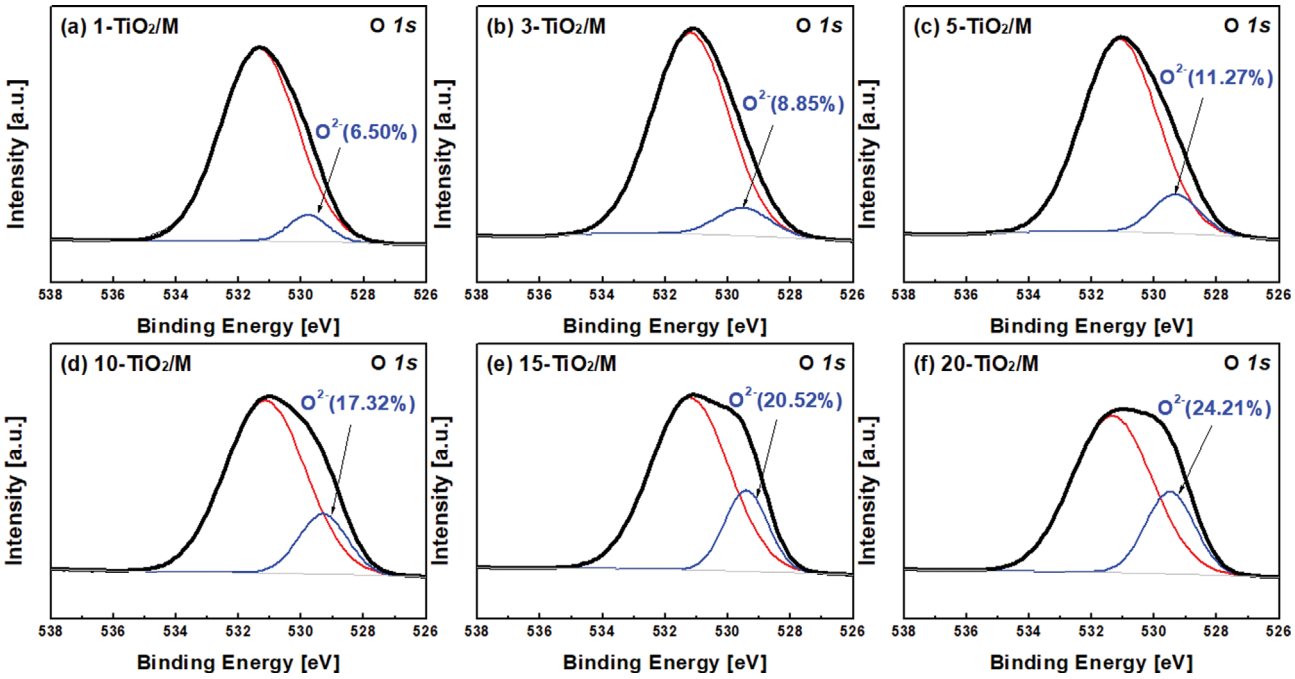

Fig. 6. Regional XPS scan for O *1s* of TiO_2/M samples.

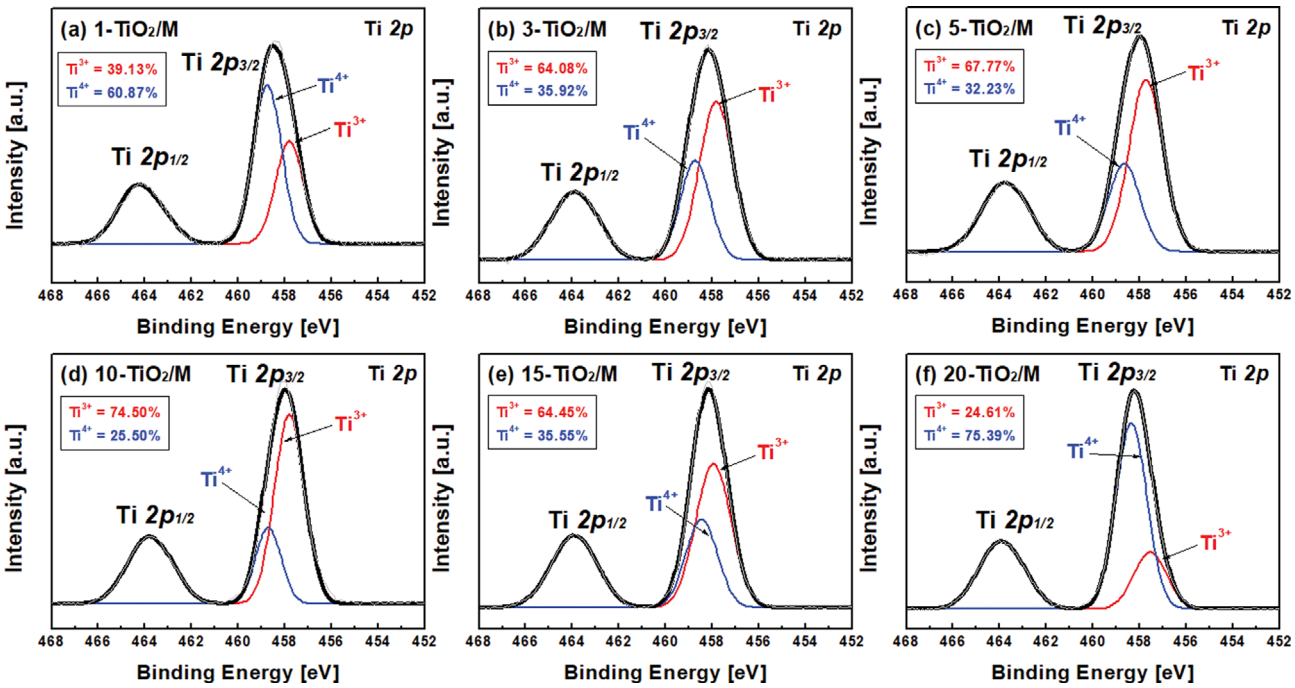

Fig. 7. Regional XPS scan for Ti *2p* of TiO_2/M samples.

eV are attributed to a combination of oxygen species in Al-O, Ca-O, Ti-OH, or titanium suboxide. Accurately deconvoluting these peaks and assigning them to specific chemical states is challenging. Nevertheless, it is evident that the bi-valence oxygen in TiO_2 increases as the TiO_2 loading amount increases, although the calculated percentages do not quantitatively or qualitatively match the amount of TiO_2 loading in TiO_2/M samples. To obtain more precise information about the chemical state of the TiO_2 loaded on TiO_2/M samples, it is necessary to investigate the local XPS scan of Ti, as shown in Fig. 7. Slight shifts of $2p_{3/2}$ and $2p_{1/2}$ to the lower binding energy were observed in TiO_2/M samples compared to the pure TiO_2 in Fig. 5, which is attributed to the interaction between TiO_2 and $Ca_{12}Al_{14}O_{33}$. The Ti $2p_{3/2}$ peaks of TiO_2/M samples were further deconvoluted into two peaks. The first peak appearing at around 457.6 eV corresponds to Ti^{3+} in Ti-OH, while the second peak at around 458.3 eV corresponds to Ti^{4+} in TiO_2. Interestingly, the peak intensity and area of Ti^{3+} increased as the TiO_2 loading amount increased up to 10-TiO_2/M and decreased at 15 and 20-TiO_2/M. This trend corresponds exactly with the NO removal efficiency, providing evidence to support the proposed assumption.

The small amount of TiO_2 loaded facilitates the supply of oxygen ions to the TiO_2 layer from the Mayenite support, and as a result, titanium hydroxide is formed on the surface with the aid of water molecules in the atmosphere. This hydroxide facilitates electron-hole separation by trapping UV light-generated holes and enhances the NO removal mechanism. This could explain the high NO removal efficiency of TiO_2/M catalyst, even with small amounts of TiO_2 loading. As confirmed, the NO removal efficiency of 5-TiO_2/M was higher than that of pure TiO_2 powder under the same conditions. When the TiO_2 loading exceeded a certain threshold (approximately 10 wt%), the additional supply of oxygen ions from the support (Mayenite) was restricted due to hindered mass transfer with the growing thickness of the TiO_2 layer. Instead, oxygen in TiO_2 form became predominant, and no further increase in NO removal efficiency was observed. Consequently, the NO removal efficiency decreased as the outer surface was covered by TiO_2 rather than Ti-OH.

CONCLUSION

Mayenite was successfully synthesized and utilized as a support for TiO_2 photocatalyst for NO removal. It was discovered that TiO_2 supported on Mayenite (TiO_2/M) outperformed pure TiO_2 powder by a significant degree. Notably, even with a small amount of TiO_2 used in the catalyst, the catalytic activity of TiO_2/M was excellent. As low as 5 wt% of TiO_2 loaded TiO_2/M showed superior NO removal efficiency compared to pure TiO_2 powder, while 10 wt% of TiO_2 loading exhibited the best catalytic performance. However, TiO_2 loading over 10 wt% resulted in a reverse trend by showing decreased catalytic activity. The enhanced catalytic activity was attributed to the unique feature of Mayenite, which provides oxygen ions to the TiO_2 layer, facilitating the formation of Ti-OH on the catalyst surface. X-ray photoelectron spectroscopy (XPS) analysis supported this theory by confirming the change of the oxidation state of oxygen along with the TiO_2 loading change on the catalyst.

ACKNOWLEDGEMENT

This work is supported by the Korea Agency for Infrastructure Technology Advancement (KAIA) grant funded by the Ministry of Land, Infrastructure and Transport (Grant: 21CTAP-C157328-02).

REFERENCES

1. K. Skalska, J. S. Miller and S. Ledakowicz, *Sci. Total Environ.*, **408**, 3976 (2010).
2. S. Roy, M. S. Hedge and G. Madras, *Appl. Energy*, **86**, 2283 (2009).
3. V. Praveena and M. L. J. Martin, *J. Energy Inst.*, **91**, 704 (2018).
4. F. Liu, S. Beirle, Q. Zhang, R. J. van der A, B. Zheng, D. Tong and K. He, *Atmos. Chem. Phys.*, **17**, 9261 (2017).
5. J. H. Lee, C. F. Wu, G. Hoek, K. de Hoogh, R. Beelen, B. Brunekreef and C. C Chan, *Sci. Total Environ.*, **472**, 1163 (2014).
6. Y. J. Kim, H. J. Kwon, I. Heo, I. S. Nam, B. K. Cho, J. W. Choung, M. S. Cha and G. K. Yeo, *Appl. Catal. B.*, **126**, 9 (2012).
7. S. Hwang, Y. Kim, J. Lee, E. Lee, H. Lee, C. Jeong, C. H. Kim and D. H. Kim, *Catal. Today*, **384**, 88 (2022).
8. J. Ângelo, L. Andrade, L. M. Madeira and A. Mendes, *J. Environ. Manage.*, **129**, 522 (2013).
9. W. Li, H. Yu, Z. Zhang, W. Hei, K. Liang and H. Yu, *J. Hazard. Mater.*, **420**, 126640 (2021).
10. C. Chitpakdee, A. Junkaew, P. Maitarad, L. Shi, V. Promarak, N. Kungwan and S. Namuangruk, *Chem. Eng. J.*, **369**, 124 (2019).
11. S. H. Seo, S. H. Jo, Y. S. Son, T. H. Kim, T. H. Kim and S. Yu, *Chem. Eng. J.*, **387**, 124083 (2020).
12. M. Chen and J. W. Chu, *J. Clean. Prod.*, **19**, 1266 (2011).
13. M. Z. Guo and C. S. Poon, *Build Environ.*, **70**, 102 (2013).
14. W. Shen, C. Zhang, Q. Li, W. Zhang, L. Cao and J. Ye, *J. Clean. Prod.*, **87**, 762 (2015).
15. J. H. Seo, H. N. Yoon, S. H. Kim, S. J. Bae, D. I. Jang, T. G. Kil, S. M. Park and H. K. Lee, *Compos. Struct.*, **33**, 68 (2020).
16. T. L. Thompson and J. T. Yates, *Chem. Rev.*, **106**, 4428 (2006).
17. K. Nagaveni, M. S. Hegde, N. Ravishankar, G. N. Subbanna and G. Madras, *Langmuir*, **20**, 2900 (2004).
18. E. V. Salomatina, D. G. Fukina, A. V. Koryagin, D. N. Titaev, E. V. Suleimanov and L. A. Smirnova, *J. Environ. Chem. Eng.*, **9**, 106078 (2021).
19. V. Tiwari, J. Jiang, V. Sethi and P. Biswas, *Appl. Catal. A-Gen.*, **345**, 241 (2008).
20. F. Haque, E. Vaisman, C. H. Langford and A. Kantzas, *J. Photochem. Photobiol. A.*, **169**, 21 (2005).
21. G. P. Lepore, L. Persaud and C. H. Langford, *J. Photochem. Photobiol. A.*, **98**, 103 (1996).
22. S. Liu, M. Lim and R. Amal, *Chem. Eng. Sci.*, **105**, 46 (2014).
23. N. Taoufik, A. Elmchaouri, F. Anouar, S. A. Korili and A. Gilb, *J. Water Process. Eng.*, **31**, 100876 (2019).
24. D. Kanakaraju, J. Kockler, C. A. Motti, B. D. Glass and M. Oelgemöller, *Appl. Catal. B.*, **166**, 45 (2015).
25. A. Yousefi, A. Allahverdi and P. Hejazi, *Constr. Build Mater.*, **41**, 224 (2013).
26. J. Li, L. Wang, C. Han, F. Su, Y. Leng and L. Ye, *Chin. J. Chem. Eng.*, **28**, 2587 (2020).

27. M. P. Nicolás, J. Balbuena, M. C. Yusta, L. Sánchez, I. N. Blasco, J. M. Fernández and J. I. Alvarez, *Cem. Concr. Res.*, **70**, 67 (2015).
28. J. Yao, Y. Zhang, Y. Wang, M. Chen, Y. Huang, J. Cao and S. C. Lee, *RSC Adv.*, **7**, 24683 (2017).
29. H. Hosono, K. Hayashi, K. Kajihara, P. V. Sushko and A. L. Shluger, *Solid State Ion.*, **180**, 550 (2009).
30. J. N. Kim, C. H. Ko and K. B. Yi, *Int. J. Hydrog. Energy*, **38**, 6072 (2013).
31. Z. S. Li, N. S. Cai, Y. Y. Huang and H. J. Han, *Energy Fuels*, **19**, 1447 (2005).
32. J. H. Park, J. J. Park, H. J. Park and K. B. Yi, *Clean Technol.*, **26**, 304 (2020).
33. I. Rhee, J. S. Lee, J. B. Kim and J. H. Kim, *Materials*, **11**, 877 (2018).
34. X. Tan, G. Qin, G. Cheng, X. Song, X. Chen, W. Dai and X. Fu, *Catal. Sci. Technol.*, **20**, 6923 (2020).
35. I. Nakamura, N. Negishi, S. Kutsuna, T. Ihara, S. Sugihara and K. Takeuchi, *J. Mol. Catal. A. Chem.*, **161**, 205 (2000).
36. H. Eskandarloo, A. Badiei and M. A. Behnajady, *Ind. Eng. Chem. Res.*, **53**, 7847 (2014).
37. R. Wang, H. Yang, Y. Lu, K. Kanamori, K. Nakanishi and X. Guo, *ACS Omega*, **2**, 8148 (2017).
38. J. F. Moulder, W. F. Stickle, P. E. Sobol and K. D. Bomben, in *Handbokk of X-ray photoelectron spectroscopy*, J. Chastain Eds., Perkin-Elmer Corporation, Eden Prarie (1992).
39. J. S. Dalton, P. A. Janes, N. G. Jones, J. A. Nicholson, K. R. Hallam and G. C Allen, *Environ. Pollut.*, **120**, 415 (2002).
40. B. Ohtani, Y. Okugawa, S. Nishimoto and T. Kagiya, *J. Phys. Chem.*, **91**, 3550 (1987).
41. Y. Oosawa and M. Grätzel, *J. Chem. Soc., Faraday Trans.*, **1**, 197 (1988).